13. J. Helbert, A. Maturilli, N. Mueller, in *Venus Geochemistry: Progress, Prospects, and New Missions* (Lunar and Planetary Institute, Houston, TX, 2009), abstr. 2010.
14. J. Helbert, A. Maturilli, *Earth Planet. Sci. Lett.* **285**, 347 (2009).
15. Coronae are circular volcano-tectonic features that are unique to Venus and have an average diameter of ~250 km (*5*). They are defined by their circular and often radial fractures and always produce some form of volcanism.
16. G. E. McGill, S. J. Steenstrup, C. Barton, P. G. Ford, *Geophys. Res. Lett.* **8**, 737 (1981).
17. R. J. Phillips, M. C. Malin, *Annu. Rev. Earth Planet. Sci.* **12**, 411 (1984).
18. E. R. Stofan, S. E. Smrekar, D. L. Bindschadler, D. Senske, *J. Geophys. Res.* **23**, 317 (1995).
19. Estimated elastic thickness values at Themis Regio are typically 10 to 20 km (*20*, *21*). The authors of (*22*) conducted a global admittance study and found values of elastic thickness of 0 to 50 km at both Dione and Themis Regiones. Their analysis also shows regions of large elastic thickness, up to 100 km, in the northern portion of Dione Regio covering Ushas Mons. Estimates of average apparent depth of compensation (ADC) for Dione and Themis Regiones are 130 km and 100 km (*21*), respectively. The elastic thickness at Imdr Regio cannot be reliably estimated due to the low resolution of the gravity field in that region (*53*). Stofan *et al*. (*18*) estimated an ADC of 260 km, which is consistent with a deep plume.
20. M. Simons, S. C. Solomon, B. H. Hager, *Geophys. J. Int.* **13**, 24 (1997).
21. S. E. Smrekar, E. R. Stofan, *Icarus* **139**, 100 (1999).
22. F. S. Anderson, S. E. Smrekar, *J. Geophys. Res. Planets* **111**, E08006 (2006).
23. S. T. Keddie, J. W. Head, *J. Geophys. Res.* **101**, 11,729 (1995).
24. E. R. Stofan, J. E. Guest, A. W. Brian, *Mapping of V-28 and V-53*, T. K. P. Gregg, K. L. Tanaka, R. S. Saunders, Eds. (U.S. Geological Society Open-File Report 2005-1271, Abstracts of the Annual Meeting of Planetary Geologic Mappers, Washington, DC, 2005), pp. 20–21.
25. E. R. Stofan, S. E. Smrekar, J. Helbert, P. Martin, N. Mueller, *Lunar Planet. Sci.* **XXXIX**, abstr. 1033 (2009).
26. B. D. Campbell *et al*., *J. Geophys. Res.* **97**, 16,249 (1992).
27. R. J. Phillips, N. R. Izenberg, *Geophys. Res. Lett.* **22**, 1617 (1995).
28. C. M. Pieters *et al*., *Science* **234**, 1379 (1986).
29. B. Fegley Jr., R. G. Prinn, *Nature* **337**, 55 (1989).
30. A. H. Treiman, C. C. Allen, *Lunar Planet. Sci. Conf.* **XXV**, 1415 (1994).
31. M. I. Zolotov, V. P. Volkov, in *Venus Geology, Geochemistry, Geophysics—Research Results from the USSR* (Univ. of Arizona Press, Tucson, AZ, 1992), pp. 177–199.
32. B. Fegley, A. H. Treiman, V. L. Sharpton, *Proc. Lunar Planet. Sci.* **22**, 3 (1992).
33. B. Fegley, K. Lodders, A. H. Treiman, G. Klingelhöfer, *Icarus* **115**, 159 (1995a).
34. B. Fegley *et al*., *Icarus* **118**, 373 (1995b).
35. A. M. Baldridge, S. J. Hook, C. I. Grove, G. Rivera, *Remote Sens. Environ.* **113**, 711 (2009).
36. L. T. Elkins-Tanton *et al*., *Contrib. Minerol. Petrol.* **153**, 191 (2007).
37. S. A. Gibson, R. N. Thompson, A. P. Dickin, *Earth Planet. Sci. Lett.* **174**, 355 (2000).
38. L. S. Glaze, *J. Geophys. Res.* **104**, 18,899 (1999).
39. *New Scientist* **23**, 52 (2009) (www.newscientist.com/article/dn17534).
40. V. S. Meadows, D. Crisp, *J. Geophys. Res.* **101**, 4595 (1996).
41. B. Fegley, *Icarus* **128**, 474 (1997).
42. E. R. Stofan, A. W. Brian, J. E. Guest, *Icarus* **173**, 312 (2005).
43. P. R. Hooper, in *Large Igneous Provinces: Continental, Oceanic and Planetary Flood Volcanism*, J. J. Mahoney, M. F. Coffin, Eds. (Monograph 100, American Geophysical Union, Washington, DC, 1997), pp. 1–28.
44. M. A. Bullock, D. H. Grinspoon, *Icarus* **150**, 19 (2001).
45. R. G. Strom, G. G. Schaber, D. D. Dawson, *J. Geophys. Res.* **99**, 10,899 (1994).
46. K. M. Roberts, J. E. Guest, J. W. Head, M. G. Lancaster, *J. Geophys. Res.* **97**, 15,991 (1992).
47. C. R. K. Kilburn, in *Encyclopedia of Volcanoes*, H. Sigurdsson, Ed. (Academic Press, San Diego, CA, 2000), pp. 291–306.
48. We have rounded these numbers in recognition that the age estimates have higher uncertainties than the volume estimates.
49. G. Choblet, E. M. Parmentier, *Phys. Earth Planet. Inter.* **173**, 290 (2009).
50. M. E. Davies *et al*., *Celestial Mech.* **39**, 103 (1986).
51. P. K. Seidelmann *et al*., *Celestial Mech. Dyn. Astron.* **82**, 83 (2002).
52. M. E. Davies *et al*., *J. Geophys. Res.* **97**, 13,141 (1992).
53. A. S. Konopliv, W. S. Banerdt, W. L. Sjogren, *Icarus* **139**, 3 (1999).
54. G. L. Hashimoto, T. Imamura, *Icarus* **154**, 239 (2001).
55. This research was carried out in part at the Jet Propulsion Laboratory, California Institute of Technology, and was sponsored by the Planetary Geology and Geophysics Program and NASA. We gratefully acknowledge the work of the entire Venus Express and VIRTIS teams. We thank the European Space Agency, Agenzia Spaziale Italiana, Centre National des Etudes Spatiales, CNRS/Institut National des Sciences de l'Univers, and the other national space agencies that have supported this research. VIRTIS is led by INAF-IASF, Rome, Italy, and LESIA, Observatoire de Paris, France.

7 January 2010; accepted 25 March 2010
Published online 8 April 2010;
10.1126/science.1186785
Include this information when citing this paper.

Cryogenian Glaciation and the Onset of Carbon-Isotope Decoupling

Nicholas L. Swanson-Hysell,[1] Catherine V. Rose,[1] Claire C. Calmet,[1] Galen P. Halverson,[2]* Matthew T. Hurtgen,[3] Adam C. Maloof[1]†

Global carbon cycle perturbations throughout Earth history are frequently linked to changing paleogeography, glaciation, ocean oxygenation, and biological innovation. A pronounced carbonate carbon-isotope excursion during the Ediacaran Period (635 to 542 million years ago), accompanied by invariant or decoupled organic carbon-isotope values, has been explained with a model that relies on a large oceanic reservoir of organic carbon. We present carbonate and organic matter carbon-isotope data that demonstrate no decoupling from approximately 820 to 760 million years ago and complete decoupling between the Sturtian and Marinoan glacial events of the Cryogenian Period (approximately 720 to 635 million years ago). Growth of the organic carbon pool may be related to iron-rich and sulfate-poor deep-ocean conditions facilitated by an increase in the Fe:S ratio of the riverine flux after Sturtian glacial removal of a long-lived continental regolith.

Throughout most of the Phanerozoic Eon [542 million years ago (Ma) to present], paired records of carbonate carbon ($\delta^{13}C_{carb}$) and coeval bulk organic carbon ($\delta^{13}C_{org}$) isotopes are consistent with a model in which the organic carbon in marine sediments is derived and fractionated from contemporaneous dissolved inorganic carbon (DIC). In contrast, $\delta^{13}C_{carb}$ and $\delta^{13}C_{org}$ records from Ediacaran (635 to 542 Ma) carbonate successions (*1*–*3*) show relatively invariant $\delta^{13}C_{org}$ during large changes to $\delta^{13}C_{carb}$ across the ~580 million-year-old Shuram-Wonoka anomaly (Fig. 1 and fig. S1). This behavior has been used to develop and support a model for the Neoproterozoic (1000 to 542 Ma) carbon cycle in which invariant $\delta^{13}C_{org}$ values result from a very large oceanic reservoir of ^{13}C-depleted dissolved organic carbon (DOC) and particulate organic carbon (POC) (or, alternatively, sourced from a large sedimentary reservoir) that overwhelms the signal from primary biomass fractionated from contemporaneous DIC (*4*). We consider the large oceanic reservoir model and, as in (*2*), use the term DOC to collectively refer to organic carbon that is truly dissolved as well as suspended colloidal organic carbon and fine POC. The buildup and maintenance of a large DOC pool implies low C_{org} remineralization—perhaps associated with low oxygen and sulfate levels—but high nutrient liberation efficiency. In such an ocean, the $\delta^{13}C$ of the DIC pool is sensitive to inputs (via remineralization) from the ^{13}C-depleted DOC pool that can drive negative excursions. The end of the invariance in the $\delta^{13}C_{org}$ record in the latter stages of the Shuram-Wonoka anomaly has been interpreted as the demise of the large DOC pool (*2*, *3*).

Stratigraphically constrained coupled records of $\delta^{13}C_{carb}$–$\delta^{13}C_{org}$ at sufficient detail to test this carbon cycle model have been available only from carbonates of Ediacaran age (*2*, *3*). We present paired $\delta^{13}C_{carb}$ and $\delta^{13}C_{org}$ data from

[1]Department of Geosciences, Princeton University, Princeton, NJ 08544, USA. [2]Geology and Geophysics, University of Adelaide Mawson Laboratories, Adelaide, SA 5005, Australia. [3]Department of Earth and Planetary Sciences, Northwestern University, Evanston, IL 60208, USA.
*Present address: Department of Earth and Planetary Sciences, McGill University, Montreal, Quebec H3A 2A7, Canada.
†To whom correspondence should be addressed. E-mail: maloof@princeton.edu

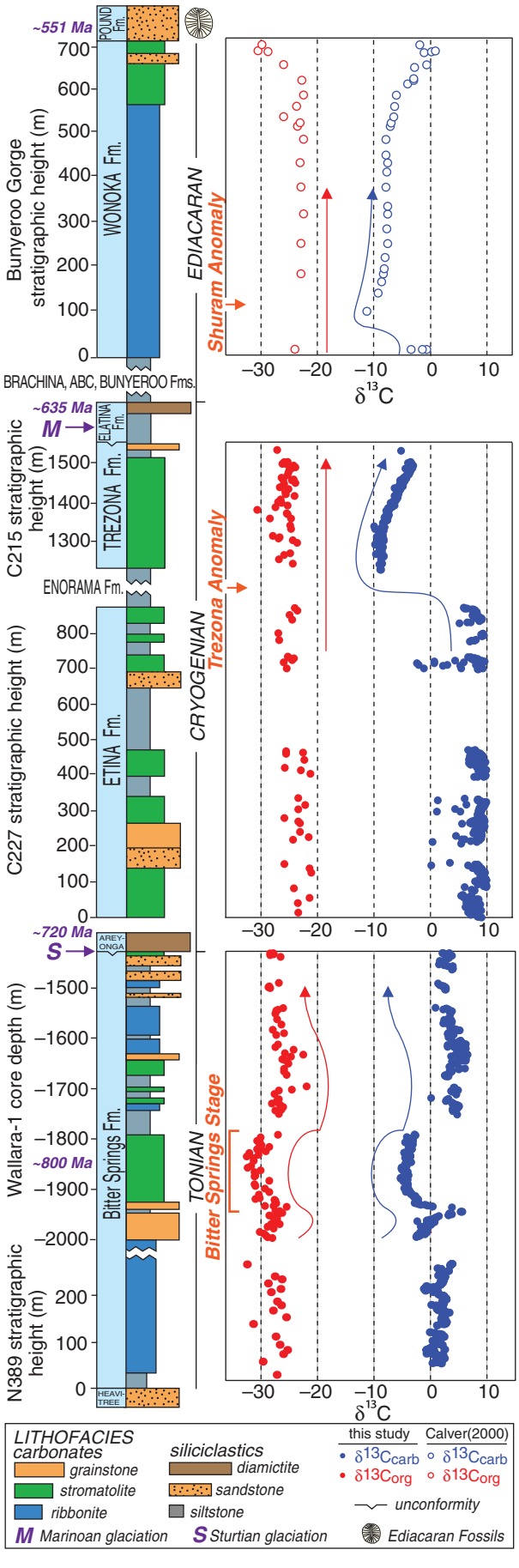

Fig. 1. Carbonate carbon isotope values and organic carbon isotope values from Neoproterozoic carbonates of Australia with simplified lithostratigraphy. The plotted lithofacies represent the lithologies that dominate each interval, with wider boxes corresponding to deposition in shallower water. N389 field-section and Wallara-1 core data are from the Bitter Springs Formation of the Amadeus Basin, deposited before the Sturtian glacial event. C227 and C215 are part of a continuous field section through the interglacial stratigraphy of the Adelaide Rift Complex. Data for the Wonoka Formation are from (*1*). The Bitter Springs, Trezona, and Shuram carbon isotope anomalies are labeled next to the carbon isotope records. The pre–Sturtian Islay anomaly is not recorded in the Bitter Springs Formation because of a disconformity at the contact with the overlying glacial sediments. The Global Boundary Stratotype Section and Point for the Cryogenian/Ediacaran Period boundary is at the contact between the glacigenic Elatina formation and the overlying Nuccaleena cap carbonate. Though it has yet to be formally defined with a stratotype section, we place the Tonian/Cryogenian boundary at the lowermost evidence for Neoproterozoic glaciation, in concurrence with the 2009 recommendation of the International Commission on Stratigraphy.

older Neoproterozoic strata: the Bitter Springs Formation of the Amadeus Basin, central Australia, that was deposited during the Tonian Period (1000 to ~720 Ma) and the Etina-Trezona Formations of the adjacent Adelaide Rift Complex deposited during the Cryogenian Period (~720 to 635 Ma) (*5*). Together with published data from the Ediacaran Wonoka Formation (*1*), also of the Adelaide Rift Complex, these records span numerous $\delta^{13}C_{carb}$ shifts throughout the Neoproterozoic Era on a single continent, enabling a test of the hypothesis that a large reservoir of DOC and corresponding invariance in $\delta^{13}C_{org}$ was a feature of the carbon cycle for the entire era.

The paired carbon isotope data from the Bitter Springs Formation demonstrate covariation across the onset of the ~800-Ma Bitter Springs stage and throughout the stage itself. At the termination of the Bitter Springs stage, $\delta^{13}C_{carb}$ values shift abruptly from –2.7 per mil (‰) to +5.3‰, whereas $\delta^{13}C_{org}$ shifts from –29.9‰ to –26.7‰ (Fig. 1). The stable isotope results are virtually identical between the 2-km-deep Wallara drill core and a surface outcrop 120 km away, indicating that the signal is basin-wide and that neither surface oxidation nor meteoric diagenesis have substantially altered the $\delta^{13}C_{carb}$–$\delta^{13}C_{org}$ record. The sympathetic shifts in $\delta^{13}C_{carb}$ and $\delta^{13}C_{org}$ across the Bitter Springs stage confirm that the stage reflects a large-scale perturbation to the isotopic composition of the DIC pool and that organic matter in the sediments is representative of coeval biomass that fixed carbon from this ^{13}C-depleted DIC (fig. S1). In stark contrast, $\delta^{13}C_{org}$ values remain invariant across the Cryogenian Trezona anomaly, in which $\delta^{13}C_{carb}$ drops by 18‰. Before the Trezona anomaly, the $\delta^{13}C_{carb}$ values of the Etina Formation plateau at ~8‰, which is similar to the values observed in Cryogenian interglacial carbonates from Namibia (*6*), Mongolia (*7*), and Scotland (*8*). After deposition of the Enorama shale, carbonates of the subtidal Trezona Formation record $\delta^{13}C_{carb}$ values of –10‰ that increase up-stratigraphy to –2‰ before the glacial sediments of the Elatina Formation. Despite these dramatic changes in $\delta^{13}C_{carb}$, $\delta^{13}C_{org}$ values remained constant at –25‰ (Fig. 1). Unlike during the Shuram-Wonoka anomaly, there was not an increase in the variability of $\delta^{13}C_{org}$ values upwards through the Trezona anomaly. The new Australian data sets do not show significant correlation between $\delta^{13}C_{org}$ and total organic carbon, a proxy that is sometimes used as evidence for alteration of the $\delta^{13}C_{org}$ signal (fig. S3). Taken together, the new data constrain the buildup of a large DOC pool to after the Bitter Springs stage of the mid-to-late Tonian but before the onset of the end-Cryogenian glaciation.

This timing for the growth of the DOC pool and the onset of non-steady-state dynamics is consistent with very low sulfate levels in the Cryogenian oceans (*9*) and a return to ferruginous conditions in the deep ocean during early

Cryogenian glaciation (*10*, *11*). In such an ocean, decreased rates of aerobic respiration and bacterial sulfate reduction would slow organic carbon remineralization and extend the residence time of DOC. Preferential remineralization of organic P over C, as occurs with increasing depth in the modern ocean (*12*), could increase the C:P ratio of DOC with the liberated phosphate, helping to sustain the productivity necessary to accumulate a large DOC pool. Furthermore, anoxic bottom-water conditions would favor burial of high C:P organic matter because of decreased burial of P bound to Fe oxyhydroxides (*13*), further maintaining nutrient supply and sustaining the primary productivity required to explain elevated Cryogenian $\delta^{13}C_{carb}$ values (*14*).

The return to ferruginous ocean conditions and the buildup of DOC can be explained as a consequence of global glaciation. The development of a thick continental regolith of unconsolidated, chemically leached debris and soil during the 1.5 billion years between the ~2.2-billion-year-old Paleoproterozoic Makganyene glaciation of South Africa (*15*) and the ~720-Ma early Cryogenian pan-glacial event (*16*) would have suppressed the Fe:S ratio of continental runoff. After reaching a depth of ~0.5 m, the thickness of regolith is inversely proportional to the weatherability of the top of bedrock (Fig. 2B) (*17*, *18*). Although the average concentrations of Fe oxides are similar between sedimentary rocks and the rest of the upper continental crust, the average concentration of S is eight times greater in sedimentary lithologies (*19*). Thus, the development of a thick regolith on continental interiors in the absence of glacial erosion and the preferential weathering of S-rich sedimentary and ophiolitic rocks on continental margins, where tectonic uplift could facilitate physical removal of regolith, would have limited relative Fe input to the ocean. This mechanism for maintaining high relative S delivery helps to explain evidence for widespread euxinic conditions through the Mesoproterozoic [1.6 to 1.0 billion years ago (*20*, *21*)].

The association of banded-iron formation (BIF) with Sturtian-age glacial deposits demonstrates that during the glaciation, Fe supply from hydrothermal and continental-weathering sources exceeded sulfide availability (*9*). This Fe input removed available oxidants, resulting in anoxia, low sulfate levels, and BIF deposition. Although the presence of BIF associated with the glaciation indicates transient ferruginous conditions, the maintenance of iron-rich deep oceans (*10*, *11*) requires that a high relative flux of Fe continued in the post-glacial period. Ubiquitous continental ice sheets during the Sturtian glaciation would have scoured continental interiors, removing the thick mantle of regolith. The relatively thick Sturtian glacial deposits may represent physical evidence of redeposited regolith that was eroded by dynamic early Cryogenian ice sheets, whereas the relatively thin Marinoan glacial deposits may reflect the activity of stable late Cryogenian ice sheets frozen to scoured bedrock—similar to the Pleistocene evolution of the Canadian Shield and Laurentide ice sheet (*22*). When ice sheets retreated during the high CO_2 escape from the early Cryogenian glaciation, the vigorous weathering of freshly exposed continental crust would result in a higher proportional delivery of Fe to S into the ocean than during the preceding 1.5 billion years. This postulated increase in the relative delivery of material derived from continental interiors as compared with continental margins is supported by a steady increase in the $^{87}Sr/^{86}Sr$ composition of the ocean after the Sturtian ice age (*23*). Because the DOC reservoir does not build up until after the Sturtian glaciation in this model, it predicts that $\delta^{13}C_{org}$ will vary across the immediately pre-Sturtian Islay negative $\delta^{13}C_{carb}$ anomaly (*8*).

The sudden post-Sturtian increase in weatherability could have led to lower equilibrium atmospheric CO_2 during the Cryogenian without changes to volcanic CO_2 input (Fig. 2C). Changes in CO_2 are connected to the evolving sensitivity of silicate weathering rates to CO_2 [weatherability (k_w)] and the varying fraction of total carbon burial that occurs as organic carbon (f_{org}) (*14*). High steady-state values of $\delta^{13}C_{carb}$ during the late Tonian have been used to argue that a high f_{org} helped lower CO_2 before glaciation (*14*). The prevalence of continental landmass at low latitude that facilitated high f_{org} may have increased k_w because of the abundance of silicate rocks associated with Grenville-age orogenic belts in tropical weathering regimes. Landscape disequilibrium associated with Bitter Springs–stage rapid true-polar wander (*24*) and increased delivery of moisture to continental interiors during the opening of incipient ocean basins as Rodinia rifted apart (*25*) would have further increased k_w. Together, these late Tonian changes would have reduced CO_2 enough to initiate Sturtian glaciation. However, it was the Sturtian glaciers themselves that scoured the continents, removing the long-lived Proterozoic regolith, greatly increasing continental weatherability, and setting up a new climatic regime with lower CO_2, a ferruginous ocean with high $\delta^{13}C_{carb}$, and a large DOC pool.

Although the close association of the Trezona anomaly below Marinoan glacial deposits has been interpreted as evidence for a causal relationship between the two (*14*), the glacioeustatic sea level fall related to Marinoan glaciation did not occur until after recovery from the most negative $\delta^{13}C_{carb}$ values. In some sections, Trezona Formation $\delta^{13}C_{carb}$ values recover to ~0‰ and are followed by more than 100 m of shallowing-upward peritidal sandstones before the first glacial deposits, further attenuating the connection between the Trezona anomaly and glaciation. If the increase in k_w and sustained high f_{org} of the Cryogenian led to global cooling and oxygen release, the Trezona anomaly could reflect oxygenation of the deep ocean and partial remineralization of the large ^{13}C-depleted DOC pool, as has been suggested for the Shuram-Wonoka anomaly. Organic carbon remineralization represents a negative climate feedback, releasing CO_2 and preventing glaciation—which is consistent with the lack of glacioeustatic change during the Trezona anomaly itself. The $\delta^{13}C_{carb}$ recovery and eventual Marinoan glaciation oc-

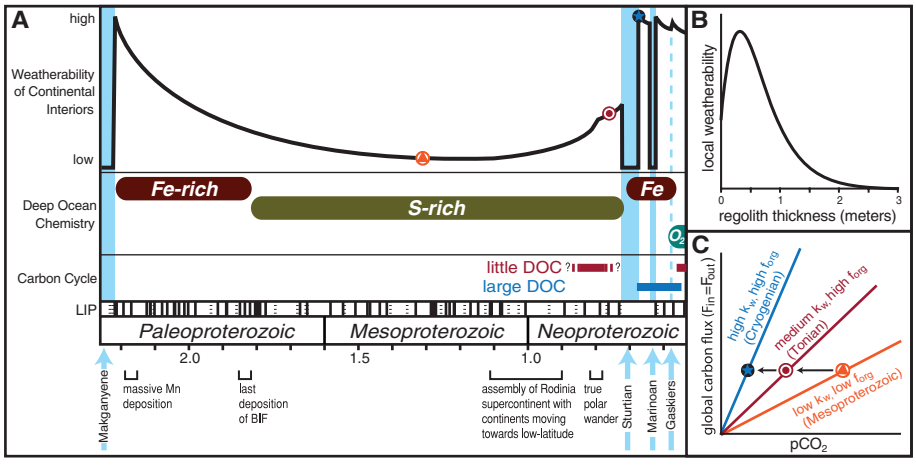

Fig. 2. (**A**) Summary illustration relating Proterozoic deep-ocean chemistry [modified from (*26*)], small versus large DOC carbon cycle, and the weatherability of continental interiors. Before the first Neoproterozoic glaciation, there was no unusual concentration of large igneous province events [shown as compiled by (*27*), with solid and dashed lines indicating <20- and >20-Ma uncertainty, respectively]. Because local weatherability is a function of regolith thickness [(**B**), modified from (*18*)], regolith development on continental interiors through the nonglacial Mesoproterozoic (*28*) would lead to the depicted decrease in regional weatherability in (A). The relationship shown schematically in (**C**) is $F_{in} = (k_w \times M_{CO_2})/(1 - f_{org})$, where k_w is the slope of the weathering-CO_2 feedback and is partly a function of the regional weatherability depicted in (B). An increase in k_w and in the relative burial of C as organic matter can result in a decrease in CO_2, as shown for the Mesoproterozoic → Tonian → Cryogenian, without changes in volcanic An increase input.

curred when the large DOC pool had been reduced in size enough to no longer represent a negative feedback to global climatic cooling.

References and Notes

1. C. R. Calver, *Precambrian Res.* **100**, 121 (2000).
2. D. A. Fike, J. P. Grotzinger, L. M. Pratt, R. E. Summons, *Nature* **444**, 744 (2006).
3. K. A. McFadden *et al.*, *Proc. Natl. Acad. Sci. U.S.A.* **105**, 3197 (2008).
4. D. H. Rothman, J. M. Hayes, R. E. Summons, *Proc. Natl. Acad. Sci. U.S.A.* **100**, 8124 (2003).
5. Data tables and methods are available as supporting material on *Science* Online.
6. G. P. Halverson, P. F. Hoffman, D. P. Schrag, A. C. Maloof, A. H. N. Rice, *Geol. Soc. Am. Bull.* **117**, 1181 (2005).
7. F. A. Macdonald, D. S. Jones, D. P. Schrag, *Geology* **37**, 123 (2009).
8. A. R. Prave, A. E. Fallick, C. W. Thomas, C. M. Graham, *J. Geol. Soc. London* **166**, 845 (2009).
9. M. T. Hurtgen, M. A. Arthur, N. Suits, A. J. Kaufman, *Earth Planet. Sci. Lett.* **203**, 413 (2002).
10. D. E. Canfield *et al.*, *Science* **321**, 949 (2008).
11. C. Li *et al.*, *Science* **328**, 80 (2010).
12. P. Sannigrahi, E. D. Ingall, R. Benner, *Geochim. Cosmochim. Acta* **70**, 5868 (2006).
13. P. Van Cappellen, E. D. Ingall, *Paleoceanography* **9**, 677 (1994).
14. D. P. Schrag, R. A. Berner, P. F. Hoffman, G. P. Halverson, *Geochem. Geophys. Geosyst.* **10**, 1029/2001GC000219 (2002).
15. R. E. Kopp, J. L. Kirschvink, I. A. Hilburn, C. Z. Nash, *Proc. Natl. Acad. Sci. U.S.A.* **102**, 11131 (2005).
16. F. A. Macdonald *et al.*, *Science* **327**, 1241 (2010).
17. F. Ahnert, Ed., *Geomorphological Models: Theoretical and Empirical Aspects* (Catena, Reiskirchen, Germany, 1987), pp. 31–50.
18. E. J. Gabet, S. M. Mudd, *Geology* **37**, 151 (2009).
19. K. H. Wedepohl, *Geochim. Cosmochim. Acta* **59**, 1217 (1995).
20. D. E. Canfield, *Nature* **396**, 450 (1998).
21. T. W. Lyons, A. D. Anbar, S. Severmann, C. Scott, B. C. Gill, *Annu. Rev. Earth Planet. Sci.* **37**, 507 (2009).
22. P. U. Clark, D. Pollard, *Paleoceanography* **13**, 1 (1998).
23. G. P. Halverson, F. O. Dudas, A. C. Maloof, S. A. Bowring, *Palaeogeogr. Palaeoclimatol. Palaeoecol.* **256**, 103 (2007).
24. A. C. Maloof *et al.*, *Geol. Soc. Am. Bull.* **118**, 1099 (2006).
25. Y. Goddéris *et al.*, *C. R. Geosci.* **339**, 212 (2007).
26. D. T. Johnston, F. Wolfe-Simon, A. Pearson, A. H. Knoll, *Proc. Natl. Acad. Sci. U.S.A.* **106**, 16925 (2009).
27. R. E. Ernst, K. L. Buchan, *Spec. Pap. Geol. Soc. Am.* **352**, 483 (2001).
28. L. C. Kah, R. Riding, *Geology* **35**, 799 (2007).

29. We thank K. Bovee, R. Levin, W. Jacobsen, L. Wingate, and L. Godfrey for assistance with sample preparation and analysis and D. Rothman, L. Kah, R. Kopp, N. Cassar, J. Higgins, J. Husson, and D. Sigman for comments and discussions. This work was supported by NSF grants EAR-0514657 and EAR-084294 to A.C.M., EAR-0720045 to M.T.H., an American Association of Petroleum Geologists Grant to C.V.R., and an NSF East Asia and Pacific Summer Institute fellowship to N.L.S.-H.

Supporting Online Material

www.sciencemag.org/cgi/content/full/328/5978/608/DC1
Materials and Methods
Figs. S1 to S4
Table S1
References

10 November 2009; accepted 11 March 2010
10.1126/science.1184508

Asian Monsoon Transport of Pollution to the Stratosphere

William J. Randel,[1]* Mijeong Park,[1] Louisa Emmons,[1] Doug Kinnison,[1] Peter Bernath,[2,3] Kaley A. Walker,[4,3] Chris Boone,[3] Hugh Pumphrey[5]

Transport of air from the troposphere to the stratosphere occurs primarily in the tropics, associated with the ascending branch of the Brewer-Dobson circulation. Here, we identify the transport of air masses from the surface, through the Asian monsoon, and deep into the stratosphere, using satellite observations of hydrogen cyanide (HCN), a tropospheric pollutant produced in biomass burning. A key factor in this identification is that HCN has a strong sink from contact with the ocean; much of the air in the tropical upper troposphere is relatively depleted in HCN, and hence, broad tropical upwelling cannot be the main source for the stratosphere. The monsoon circulation provides an effective pathway for pollution from Asia, India, and Indonesia to enter the global stratosphere.

The Asian summer monsoon circulation contains a strong anticyclonic vortex in the upper troposphere and lower stratosphere (UTLS), spanning Asia to the Middle East. The anticyclone is a region of persistent enhanced pollution in the upper troposphere during boreal summer, linked to rapid vertical transport of surface air from Asia, India, and Indonesia in deep convection, and confinement by the strong anticyclonic circulation (*1*–*6*). A mean upward circulation on the eastern side of the anticyclone extends the transport into the lower stratosphere, as evidenced by satellite observations of water vapor (*7*) and ozone (*8*), plus carbon monoxide and other pollution tracers (*1*, *4*, *5*). Model calculations have suggested that transport from the monsoon region could contribute substantially to the budget of stratospheric water vapor (*8*, *9*), but this effect has not been isolated from broader-scale tropical upwelling in observational data.

Hydrogen cyanide (HCN) is produced primarily as a result of biomass and biofuel burning and is often used as a tracer of pollution originating from fires (*10*–*12*). In the free atmosphere,

[1]National Center for Atmospheric Research, Boulder, CO, USA. [2]Department of Chemistry, University of York, Heslington, UK. [3]Department of Chemistry, University of Waterloo, Waterloo, Ontario, Canada. [4]Department of Physics, University of Toronto, Toronto, Ontario, Canada. [5]School of GeoSciences, University of Edinburgh, Edinburgh, UK.

*To whom correspondence should be addressed. E-mail: randel@ucar.edu

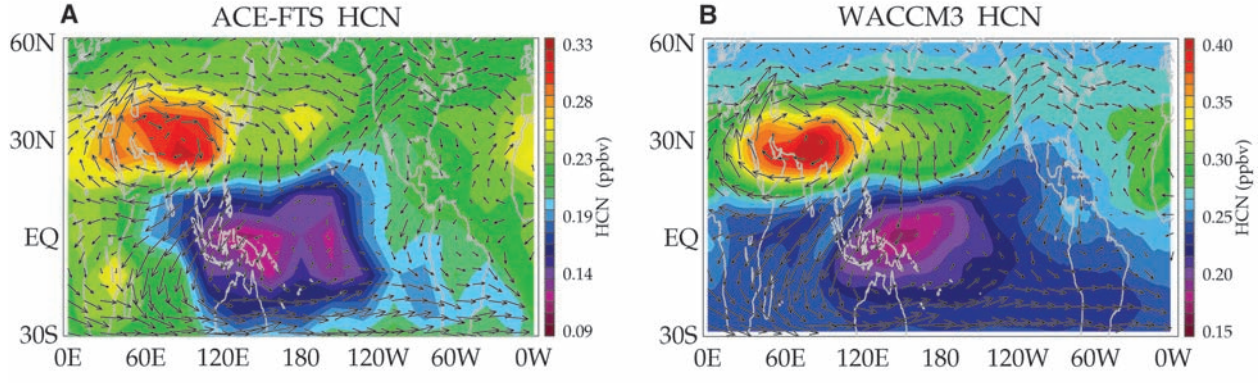

Fig. 1. Time average mixing ratio [parts per billion by volume (ppbv)] of HCN near 13.5 km during boreal summer (June to August) derived from (**A**) ACE-FTS observations and (**B**) WACCM chemical transport model calculations. Arrows in both panels denote winds at this level derived from meteorological analysis, showing that the HCN maximum is linked with the upper tropospheric Asian monsoon anticyclone.